frontiers in Agronomy

TYPE Original Research
PUBLISHED 05 August 2026
DOI 10.3389/fagro.2026.1885332

OPEN ACCESS

EDITED BY
Antonio Rafael Sánchez-Rodríguez,
University of Cordoba, Spain

REVIEWED BY
Hong Lu,
Zhejiang University, China
Iryna Loginova,
University of Tübingen, Germany
Ravi Saini,
Indian Space Research Organisation,
Hderabad, India

*CORRESPONDENCE
Katrin Kuka
katrin.kuka@julius-kuehn.de

RECEIVED 19 May 2026
REVISED 01 July 2026
ACCEPTED 06 July 2026
PUBLISHED 05 August 2026

CITATION
Kuka K, Schmitt Rahner M, Keßeler P, Kratz S and Bloem E (2026) Perennial ryegrass responses to contrasting phosphorus fertilizer sources: nutrient dynamics and root system architecture assessed by X-ray micro-computed tomography.
Front. Agron. 8:1885332.
doi: 10.3389/fagro.2026.1885332

Perennial ryegrass responses to contrasting phosphorus fertilizer sources: nutrient dynamics and root system architecture assessed by X-ray micro-computed tomography

Katrin Kuka*, Mayka Schmitt Rahner, Paul Keßeler, Sylvia Kratz and Elke Bloem

Julius Kühn-Institute (JKI), Institute for Crop and Soil Science, Braunschweig, Germany

Introduction: Although recycled phosphorus (P) fertilizers may contribute to circular nutrient management, their agronomic performance depends on how nutrient release dynamics align with plant demand, which affects biomass production and root development.

Methods: In a two-cut pot experiment with *Lolium perenne* grown in a P-poor sandy substrate, we compared an unfertilized control (P0), struvite (STR - a recycled P fertilizer), and triple superphosphate (TSP - a highly soluble mineral P source) with respect to P supply. We assessed dry matter yield, nutrient uptake, plant nutrient status, forage quality, and root system architecture, the latter examined using non-destructive X-ray micro-computed tomography.

Results: Treatment responses were strongly time-dependent. In the first cut, STR produced a significantly higher dry matter yield than P0 (2.22 vs. 1.87 t ha^{-1}), while not differing significantly from TSP, despite having a lower nitrogen (N) concentration and uptake than P0 and TSP. These results suggest a temporal dissociation between early biomass formation and N acquisition, which may partly reflect differences in N source and availability between treatments. STR also increased P uptake relative to the P0 treatment (7.74 vs. 6.25 kg ha^{-1}), though values remained below those of TSP (9.41 kg ha^{-1}). In contrast, TSP promoted stronger early root development, as evidenced by greater total root volume and greater root surface area in coarser diameter classes than P0. STR, however, showed reduced fine-root volume compared to P0. By the second cut, nutrient concentrations declined across treatments. Differences in P uptake between STR and TSP decreased, and most root traits converged. Across both cuts, root volume and surface area remained concentrated in the upper substrate layers.

Conclusion: The results demonstrate that STR effectively functions as a recycled P fertilizer, supporting high initial biomass production and improved P acquisition relative to P0. Notably, its response pattern differs from that of TSP, characterized by slower nutrient delivery, weaker regrowth, and less pronounced early root proliferation.

KEYWORDS

nutrient dynamics, perennial ryegrass, phosphorus fertilization, recycled phosphorus fertilizer, root system architecture, X-ray micro-computed tomography

1 Introduction

Agricultural systems in the Baltic Sea region face increasing pressure to reduce nutrient surpluses, particularly N and P, which contribute substantially to eutrophication and the degradation of aquatic ecosystems (HELCOM, 2021). Reducing nutrient losses while maintaining agricultural productivity requires closing nutrient cycles and implementing fertilization strategies that are both agronomically effective and environmentally sound (McConville et al., 2015).

A particular focus is placed on P fertilization. P is an essential macronutrient for plant growth but is predominantly derived from non-renewable phosphate rock, exposing the European Union to supply risks and geopolitical vulnerabilities (Cordell et al., 2009; Withers et al., 2014). Therefore, recycling P from residual streams can enhance nutrient sovereignty while reducing environmental impacts. Among recycled nutrient fertilizers (RNF), struvite (magnesium ammonium phosphate hexahydrate, $MgNH_4PO_4{\cdot}6H_2O$) has gained increasing attention recently. Struvite, hereafter referred to as STR, is a crystalline mineral recovered from wastewater streams via controlled precipitation and it is characterized by low water solubility, resulting in a gradual release of plant-available P (Kratz et al., 2019; Deinert et al., 2023; Yan et al., 2025). In contrast, triple superphosphate (TSP), a widely used conventional P fertilizer, is highly water-soluble and provides readily available P shortly after application.

Beyond fertilizer chemistry, the way in which plant root systems respond plays a decisive role in determining P acquisition. As P is highly immobile in soil, its uptake primarily depends on root-mediated soil exploration rather than mass flow (Lynch and Brown, 2008). Reduced P availability induces pronounced changes in root system architecture, including increased allocation of biomass belowground, greater total root length, enhanced root surface area, finer root diameters, and intensified exploration of the topsoil (Hill et al., 2006; Lynch, 2011; Chen et al., 2018). These traits are commonly referred to as adaptive "root phenes" that collectively enhance P acquisition under nutrient limitation (Lynch, 2011, 2019).

In grasses and other fibrous-rooted species, P limitation predominantly triggers morphological rather than physiological acquisition strategies. Numerous studies have shown that increased root length density, higher specific root length, and greater overall root system size are the primary mechanisms by which grasses compensate low P availability (Lyu et al., 2016; Ros et al., 2018; Waddell et al., 2017; Wu et al., 2021). The relative contributions of morphological and physiological acquisition strategies, including rhizosphere exudation and mycorrhizal associations, vary with soil conditions, crop species, and nutrient status (Shen et al., 2018; Wen et al., 2019; Gao et al., 2023). Notably, enhanced root development under low P supply does not necessarily translate into higher shoot P concentrations or biomass production, but reflects a compensatory shift in carbon allocation aimed at maintaining nutrient uptake (Hammond and White, 2008; van Nguyen and Stangoulis, 2019).

Root system architecture is therefore a sensitive indicator of P availability and fertilization strategy. Studies comparing soluble and slowly available P sources have demonstrated that differences in the temporal P availability can substantially modify root growth patterns and spatial root distribution, even when aboveground biomass responses remain small (Ahmed et al., 2016). Consequently, the agronomic performance of recycled P fertilizers cannot be fully assessed based on yield alone, it also requires explicit consideration of belowground traits that govern nutrient acquisition.

Advances in non-destructive imaging techniques have enabled detailed analysis of root system architecture in soil. X-ray micro-computed tomography (µCT) allows the three-dimensional quantification of root volume, surface area, diameter distribution, and spatial root distribution in undisturbed substrates, thereby, overcoming the limitations of destructive root washing methods (Mooney et al., 2012; Kuka et al., 2013; Koebernick et al., 2014). In addition to root morphological parameters, X-ray µCT enables the simultaneous assessment of soil structural properties such as pore size distribution, connectivity, and root–soil contact, thereby providing an integrated perspective on plant–soil interactions (Bengough et al., 2006; Teramoto et al., 2020). Recent field and pot studies have further shown that fertilization intensity and nutrient availability strongly influence root development and root–soil interactions, with unfertilized or low-input systems often exhibiting more extensive root systems as a compensatory response to nutrient limitation (Kuka and Joschko, 2024). Despite these methodological advances, X-ray µCT has not yet been applied to directly compare root system architecture responses to contrasting P fertilizer sources, including recycled fertilizers such as struvite. The integration of µCT-derived root traits with aboveground agronomic and forage quality data across multiple harvest dates therefore represents a methodological and thematic gap in the current literature on recycled P fertilizers.

In grassland systems, however, fertilizer performance is not determined by biomass production and nutrient uptake alone, but also by its effects on forage quality. In perennial ryegrass (*Lolium perenne*), forage quality is strongly influenced by regrowth stage and plant maturity, with crude protein and digestibility declining and crude fiber concentrations increasing as development progresses. Mineral concentrations may additionally fall short of the requirements of lactating dairy cows, particularly in more mature forage. Fertilizer-induced changes in nutrient availability may therefore affect not only biomass production and plant nutrient status, but also the feeding value of the harvested forage (Castro-Hernández et al., 2017; Poetsch et al., 2016). Yet, to our knowledge, no study has systematically examined how contrasting P fertilizer sources influence forage quality parameters in perennial ryegrass across multiple cuts.

The objective of this study was to assess the effects of different P fertilization strategies (STR, TSP, and a P-free control) on the growth, nutrient dynamics, forage quality, and root system architecture of *Lolium perenne* in a controlled pot experiment conducted with a homogenized sandy substrate developed at the Institute for Crop and Soil Science at the Julius Kühn Institute (JKI). Aboveground responses were quantified by measuring dry matter (DM) yield at two cuts, phenological development (BBCH-scale), N and P uptake, shoot nutrient concentrations (N, P, K, Mg, S, Fe, Mn, Cu, Zn, B), and forage quality parameters determined by near-infrared reflectance spectroscopy (NIRS), including crude protein

(CP), crude fiber (CF), water-soluble carbohydrates (WSC), and enzymatic digestibility of organic matter (ELOS). Belowground responses were characterized non-destructively using X-ray µCT, which enabled three-dimensional (3D) quantification of root volume, root surface area, their distribution across diameter classes, and vertical root distribution within the pot profile.

Based on the contrasting nutrient supply conditions created by highly soluble TSP, slowly soluble STR, and the absence of P fertilization in the control treatment (P0), as well as the importance of root-mediated nutrient acquisition in grasses, we tested the following hypotheses:

i. chemical P binding form and the absence of P fertilization in P0 induce treatment-specific differences in aboveground plant development and productivity, including phenological development, DM yield, and nutrient uptake, due to differences in the availability of P, N, and Mg;
ii. treatment-specific nutrient supply results in differences in plant nutrient status and, consequently, in forage quality among TSP, STR, and P0;
iii. root system development and vertical root distribution respond to treatment-specific nutrient supply, as plants adjust root growth and spatial foraging in order to improve nutrient acquisition.

By integrating above- and belowground responses across two cuts and applying X-ray µCT-based root phenotyping, this study provides, to our knowledge, the first systematic comparison of µCT-derived root traits between struvite and a conventional P fertilizer in a managed grass system, combined with a multi-parameter assessment of forage quality across two harvest dates. Using *Lolium perenne* as a model, it thereby contributes to assessing the potential of struvite as a sustainable alternative to conventional mineral P fertilizers for grassland systems.

2 Materials and methods

2.1 Pot experiment with phosphorus fertilization treatments

For the pot experiment, a standardized, low-phosphorus (13.6 mg CAL-P kg^{-1}, VDLUFA soil test P level A) growth substrate was prepared consisting of 88% coarse quartz sand (0.7–1.2 mm), 10% fine calcium bentonite and 2% bark humus (0–6 mm). The pH of the substrate was adjusted to 6.3 by adding 0.837 g $CaCO_3$ per pot (corresponding to 335 mg Ca). This mixture provided a low inherent nutrient supply while ensuring adequate water retention and structural stability, and was specifically selected to ensure that P availability would be the primary yield-limiting factor. Each 1.4 L pot was filled with 2000 g of the homogenized substrate. Three phosphorus treatments were established: struvite (STR; SF-Soepenberg GmbH), triple superphosphate (TSP), and a non-fertilized control (P0). Based on the expected P uptake (above ground DM yield from a previous experiment multiplied with optimum P concentration in plant tissue), the target rate was 42 mg P per pot (representing 85% of optimum supply, aiming to accelerate treatment differentiation and shorten trial duration). This corresponds to approximately 25 kg P ha^{-1} when scaled to field rate based on the pot surface area (diameter 14.5 cm). Based on total phosphorus concentrations, 368 mg struvite (223 kg ha^{-1}, 11.4% P) and 195 mg TSP (118 kg ha^{-1}, 21.5% P) were applied per pot. Both fertilizers were finely ground prior to application and thoroughly mixed into the entire substrate volume to ensure uniform distribution. Following phosphorus incorporation, pots were incubated for two weeks in an outdoor greenhouse without plants. During this period, soil moisture was maintained at approximately 70% of maximum water holding capacity. Pots were covered with translucent plastic film to reduce evaporative losses while still allowing light to penetrate. This incubation phase allowed the initial fertilizer dissolution and equilibration within the substrate.

On May 27, 2024, each pot was sown with 22 seeds of perennial ryegrass (*Lolium perenne*). The seeding density was derived from a target rate of 1200 seeds m^{-2}, corrected for a germination capacity of 93% and adjusted to the pot surface area. At sowing, a single multi-nutrient solution was applied, aiming to provide the test crop with a sufficient supply of all essential nutrients (except P) in slight excess, ensuring that only P was yield-limiting. Target nutrient rates were based on expected DM yield from a previous experiment. Each pot received 300 mg N (equivalent to 182 kg N ha^{-1}), 292 mg K (177 kg K ha^{-1}), 30 mg S (18 kg S ha^{-1}) and 30 mg Mg (18 kg Mg ha^{-1}). The liquid N dose in the STR treatment was reduced by 15.6 mg per pot (approximately 9.5 kg N ha^{-1}) to account for the ammonium-N present in struvite, while total N supply remained 300 mg per pot (182 kg N ha^{-1}) across all treatments; no additional Mg was applied because struvite ($MgNH_4PO_4{\cdot}6H_2O$) already supplied sufficient Mg. Based on published data for powdered struvite incorporated into soil (Lunt et al., 1964; Watson et al., 2019), N and Mg from STR were assumed to be equally plant-available as the liquid fertilizer forms applied in P0 and TSP. TSP contains approximately 17% Ca, contributing approximately 33 mg Ca per pot. However, since Ca supply was not a primary focus of this study, and given that due to the pH adjustment, the substrate already contained 335 mg Ca per pot, no extra Ca was supplied with the basal nutrient solution. In addition, all pots received a micronutrient solution providing 10 mg Fe, 1 mg Mn, 1 mg Zn, 0.5 mg B, 0.2 mg Cu and 0.1 mg Mo per pot. The experiment comprised five replicates per treatment (P0, STR, TSP) and was arranged in a randomized block design within the outdoor greenhouse to minimize positional and edge effects. Throughout the experiment duration, irrigation was performed exclusively with deionized water to avoid uncontrolled nutrient inputs. No additional nutrients were applied after the first cut.

2.2 Biomass analysis

The phenological development of the plants was monitored weekly using the BBCH scale from 5 June 2024 onwards, resulting in eight observation dates in total. Aboveground biomass harvests were conducted on 2 July (cut 1, 36 days after sowing (DAS)) and 24 July (cut 2, 58 DAS) 2024, at a cutting height of 3 cm. Fresh biomass was weighed immediately after harvest. Subsamples of the fresh biomass were used to determine DM by oven-drying at 105 °C until a constant weight was achieved. For further analyses, the remaining plant material was dried at 60 °C to preserve its chemical integrity. The dried biomass was

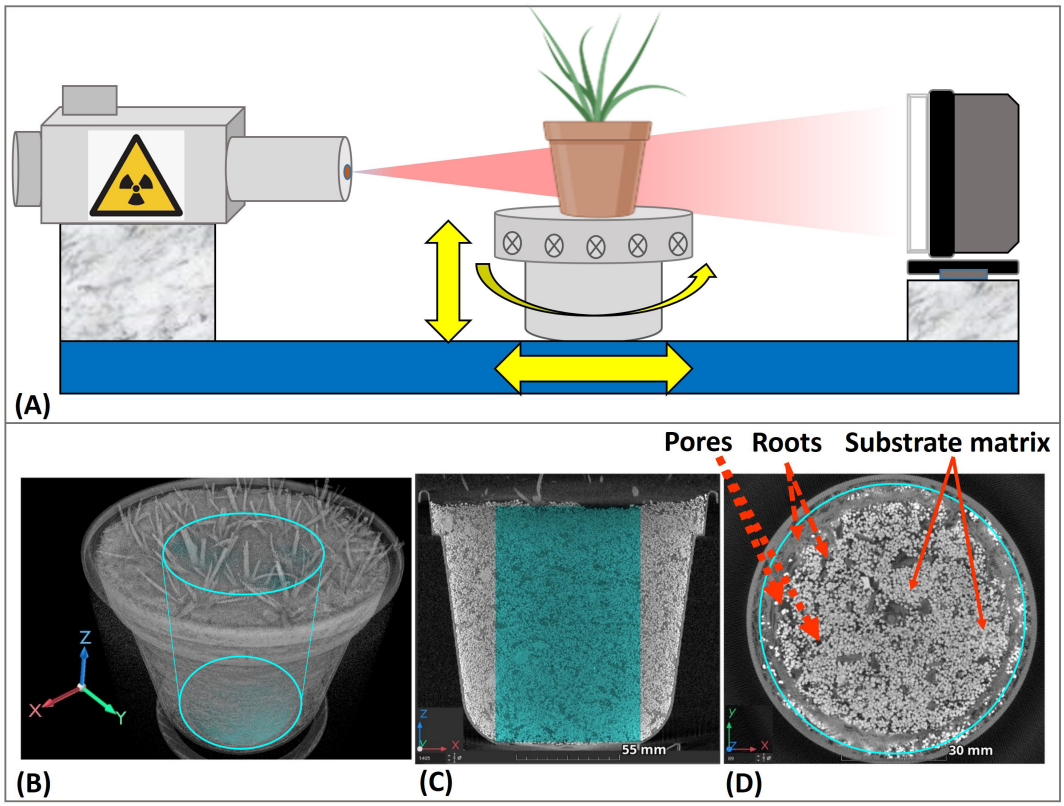

FIGURE 1
Schematic setup of the X-ray µCT imaging system **(A)**, showing the X-ray source (left), the 360° rotatable stage holding the pot with the plant–substrate sample (center), and the flat panel detector (right). Panels **(B–D)** present the reconstructed dataset: **(B)** three-dimensional volume rendering, **(C)** vertical cross-sectional view, and **(D)** horizontal cross-sectional view. The blue cylinder indicates the analyzed cylindrical region of interest.

ground to a particle size of less than 1 mm using a centrifugal mill (Retsch ZM 200). Total carbon (C) and N concentrations were determined using an elemental analyzer (Vario MAX cube CN, Elementar Analysensysteme GmbH, Germany). For multi-element analysis, microwave-assisted acid digestion was employed. To enable high-throughput liquid sample preparation for elemental analysis, 0.5 g of the dried, ground material was pre-wetted with 1.5 ml of deionized water, before being digested with 6 ml of HNO_3 and 1.5 ml of H_2O_2 in a CEM Mars 5 Xpress microwave digestion system (1600 W for 30 minutes at up to 200 °C). Elemental concentrations in the plants were then measured using inductively coupled plasma optical emission spectrometry (ICP-OES) with a Thermo iCAP 6300 Duo. In addition, forage quality parameters were assessed by near-infrared reflectance spectroscopy (NIRS) using a Foss NIRSystems 5000 spectrometer (Foss GmbH, Hamburg, Germany) with a wavelength range of 1100 to 2498 nm and a 2 nm resolution. Spectral measurements were performed on dried and ground samples, and calibration models were used to predict the following parameters: crude protein (CP), crude fiber (CF), water-soluble carbohydrates (WSC), and enzymatic digestibility of organic matter (ELOS).

2.3 X-ray µCT scanning, 3D reconstruction and image processing

Undisturbed samples were scanned in their original pots (13 cm height, 14.5 cm top diameter, 10 cm bottom diameter) immediately after each harvest using an industrial X-ray µCT system (RayScan Smart, RayScan Technologies GmbH, Meersburg, Germany). The X-ray µCT experimental setup (Figure 1A) consisted of an X-ray source, a rotatable sample stage, and a flat panel detector. A total of 720 scan projections over a full 360° rotation at 149 kV and 146 µA with an exposure time of 499 ms, resulting in a voxel resolution of 62.2 µm. No beam-hardening filter was applied. Reconstruction of the 3D volumes (*.rec) was carried out using RayWare5-Reco software.

The reconstructed 3D volume data were imported into VGStudio Max 2024.2.1 for visualization, segmentation, and quantification of root system architecture, including root volume and surface area, to assess treatment-specific effects. From the reconstructed volumes, a cylindrical region of interest (ROI) was digitally extracted for each sample (Figures 1B–D). Segmentation of pores, roots, and solid matrix was performed using a global thresholding approach based on 8-bit grayscale histograms (gray values ranging from 0 to 255). Threshold values were defined separately for each cut, with pore and solid phases segmented at < 90 and > 130 for first cut, and < 95 and > 140 for second cut, respectively. To ensure consistency and minimize operator subjectivity, an average-based global threshold value was calculated from operator-determined threshold values assessed individually for the upper, middle, and lower regions of each sample, and applied uniformly across all 15 samples within each cut dataset. The thresholds were defined separately for each cut because the use of a different sample holder for the second cut caused a slight shift in the grayscale

TABLE 1 Phenological development of *Lolium perenne* under different phosphorus fertilization treatments (P0, STR, TSP) at different days after sowing (DAS), assessed using the BBCH scale.

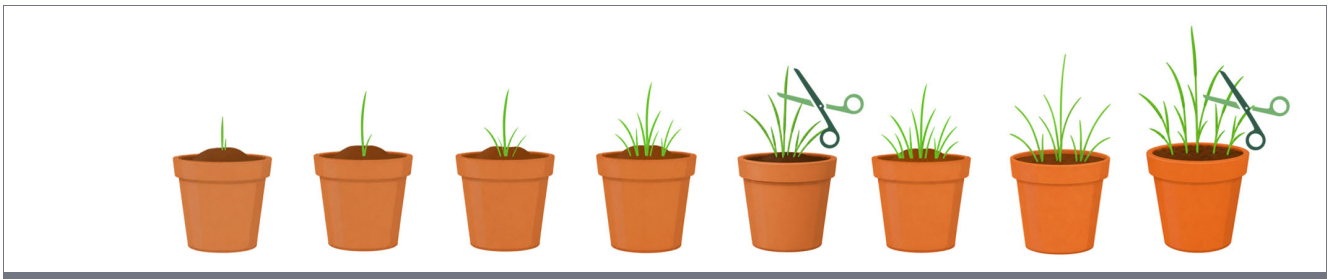

Treatment	DAS 9	DAS 16	DAS 22	DAS 30	DAS 36	DAS 44	DAS 51	DAS 58
P0	9	10	21	21-23	26	26	26-27	27
STR	9	10	21	22-24	24-25	26	27-28	27-28
TSP	9	10	21	22-24	24-25	25-26	25-27	27

DAS, days after sowing.

histogram, while remaining consistent across all samples within each cut. Subsequently, spatial transformations were applied to enhance the extraction of root structures from intermediate gray values between pore and solid phases. To quantify root volume and surface area across root thickness classes, root networks were separated into individual objects using the Foam Structure Analysis Module in VGStudio Max, configured for 3D analysis with a merge threshold of 5%. The resulting object-based dataset was used to derive root diameter classes. The detailed workflow is provided in Schmitt Rahner and Kuka (in preparation).

2.4 Statistical analyses

All statistical analyses were performed using R (version 4.5.2) in RStudio (version 2026.01.0 + 392). Data processing and visualization were conducted using the *tidyverse* collection of R packages (Wickham et al., 2019). Treatment effects on agronomic parameters (DM yield, nutrient concentrations, nutrient uptake, and forage quality parameters) as well as root traits derived from X-ray µCT were analyzed separately for each cut. In addition, cumulative values across both cuts were evaluated where appropriate. Prior to statistical analysis, data were screened for plausibility and extreme values. Outliers were identified based on graphical inspection (boxplots and residual diagnostics) and model-based evaluation using the package *DHARMa* (Hartig, 2016). Observations classified as extreme and biologically implausible were excluded from further analysis. The number of removed values was very low and did not affect the overall data structure. For inferential analysis, linear mixed-effects models were fitted using the package *glmmTMB* (McGillycuddy et al., 2025), with treatment as a fixed factor and block (replication) as a random effect to account for the experimental design. Depending on the distributional properties of the response variables, appropriate error distributions were applied; Gamma distributions with log-link were used for strictly positive and skewed data, while Gaussian models were applied to approximately normally distributed variables. Model assumptions were evaluated by visual inspection of residuals and simulation-based diagnostics using *DHARMa*. Pairwise comparisons among treatments were conducted using estimated marginal means, implemented in the R package *emmeans* (Lenth, 2023), followed by Tukey's honestly significant difference (HSD) test. Statistical significance was assessed at $p < 0.05$. Micronutrient concentrations were evaluated descriptively, as all treatments received identical micronutrient fertilization and the focus was on temporal dynamics rather than treatment effects. Results are therefore presented as means ± standard deviations without formal statistical testing. Vertical root profiles (root volume and root surface along the soil depth) were analyzed descriptively by calculating mean values per depth increment. These profiles are presented as continuous depth distributions to illustrate spatial patterns of root allocation. Variability among replicates is indicated graphically, but no formal statistical testing was applied due to the depth-resolved structure of the data and the focus on pattern interpretation.

3 Results

3.1 Classical agronomic parameters

3.1.1 Phenological development (BBCH-scale)

Phenological development was largely synchronized among the treatments until the first cut (Table 1), with only minor differences becoming apparent shortly beforehand, when P0 tended to be slightly less advanced. Following cutting, P0 showed a faster regrowth and quickly caught up with the fertilized treatments. During the later regrowth phase, development was again largely similar across all treatments, with a slight tendency for STR to reach more advanced stages toward the end.

3.1.2 Dry matter yield, nitrogen and phosphorus uptake

P fertilization, including its absence in the control treatment, significantly affected DM yield, but the direction of treatment effects

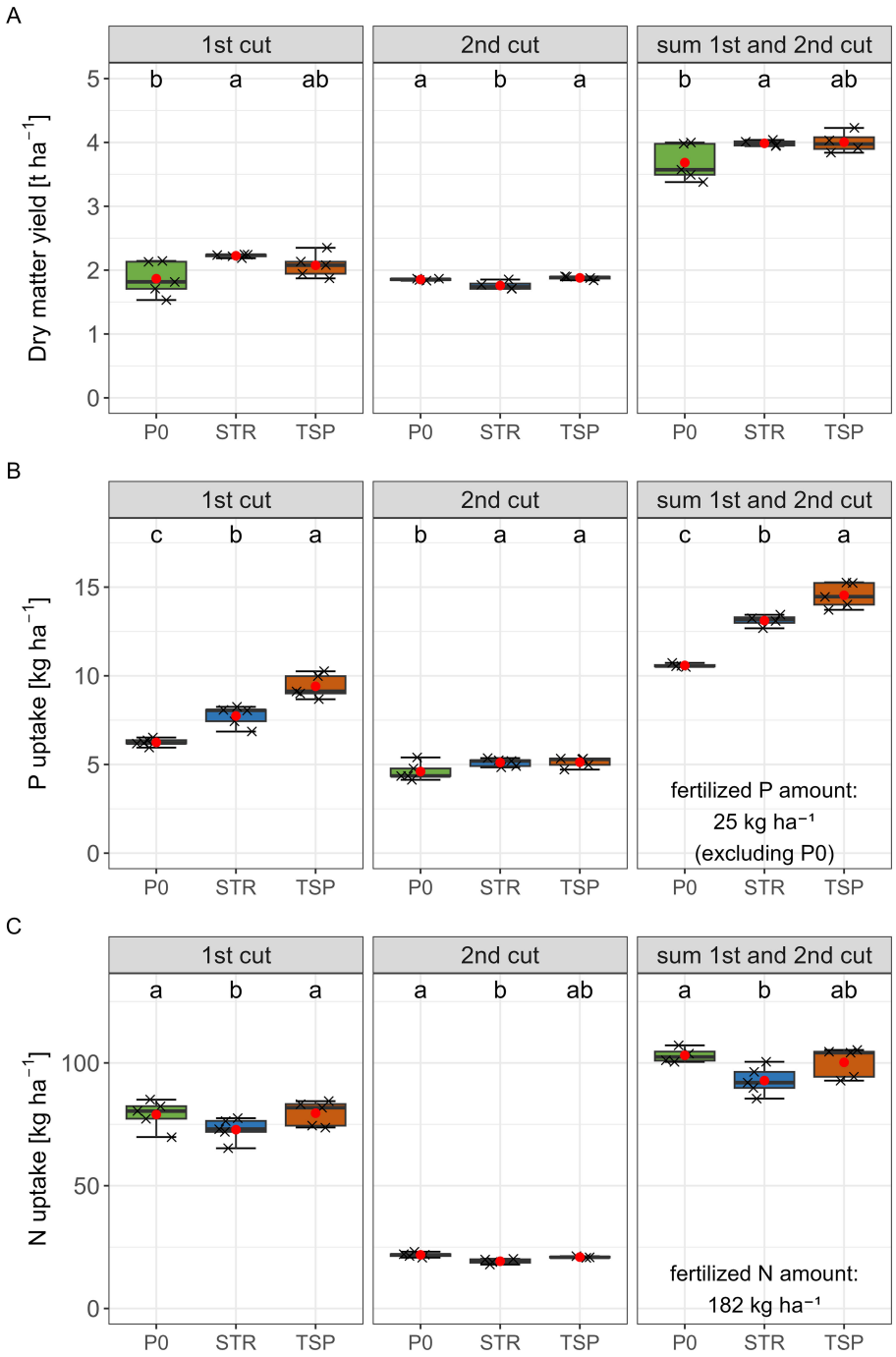

FIGURE 2
Effects of phosphorus (P) fertilization treatments, including an unfertilized control, on **(A)** dry matter (DM) yield, **(B)** phosphorus (P) uptake, and **(C)** nitrogen (N) uptake in the first cut, second cut, and the cumulative sum of both cuts. Treatments comprised P0 (no P fertilization), struvite (STR), and triple superphosphate (TSP). Boxplots show medians, interquartile ranges, and minimum–maximum values; individual symbols represent replicate observations. Red dots indicate treatment means. Different lowercase letters denote significant differences among treatments within each cut and cumulative sum according to Tukey's HSD test ($p < 0.05$).

changed between cuts (Figure 2). In the first cut, STR (2.22 ± 0.02 t ha^{-1}) produced significantly higher DM yield than P0 (1.87 ± 0.27 t ha^{-1}), while TSP (2.07 ± 0.19 t ha^{-1}) occupied an intermediate position and did not differ significantly from either treatment. In the second cut, this pattern shifted: STR (1.72 ± 0.10 t ha^{-1}) showed significantly lower DM yield than P0 (1.82 ± 0.08 t ha^{-1}) and TSP (1.80 ± 0.17 t ha^{-1}), whereas the latter two did not differ significantly from each other. When both cuts were combined, cumulative DM yield remained significantly higher under STR (3.95 ± 0.09 t ha^{-1}) than under P0 (3.68 ± 0.29 t ha^{-1}), while TSP (3.88 ± 0.32 t ha^{-1}) again showed intermediate values. Thus, the high yield advantage of STR in the first cut was not maintained during regrowth, but it was sufficient to keep total yield above the unfertilized control.

A more consistent treatment ranking was observed for P uptake (Figure 2B), despite a strong decline in magnitude from the first to the second cut. In the first cut, P uptake differed significantly among all

treatments and followed the order P0 (6.25 ± 0.21 kg ha^{-1}) < STR (7.74 ± 0.58 kg ha^{-1}) < TSP (9.41 ± 0.67 kg ha^{-1}). This ranking closely reflected the contrasting P supply conditions, with no P fertilization in P0 and an identical fertilized P amount of 25 kg ha^{-1} in STR and TSP, but with greater short-term plant availability under the readily soluble TSP treatment. In the second cut, overall P uptake was substantially lower and treatment separation decreased; P0 (4.60 ± 0.50 kg ha^{-1}) remained significantly lower than STR (5.11 ± 0.22 kg ha^{-1}) and TSP (5.13 ± 0.28 kg ha^{-1}), whereas STR and TSP no longer differed significantly from each other. Despite this partial convergence, cumulative P uptake across both cuts still showed a fully separated pattern, again following P0 (10.85 ± 0.60 kg ha^{-1}) < STR (12.85 ± 0.66 kg ha^{-1}) < TSP (14.54 ± 0.70 kg ha^{-1}) with significant differences among all treatments. Thus, the same total P input in STR and TSP translated into markedly different early and cumulative P uptake patterns, whereas DM yield responses showed a less consistent treatment ranking across cuts.

P utilization efficiency (PUE), expressed as DM yield per unit of plant P uptake, differed significantly among treatments and showed contrasting temporal patterns. In the first cut, PUE was significantly higher under P0 (299.6 ± 49.5 kg DM kg^{-1} P) and STR (289.1 ± 24.7 kg DM kg^{-1} P) than under TSP (222.1 ± 32.5 kg DM kg^{-1} P), indicating that the higher P uptake under TSP was not proportionally reflected in greater biomass production. In the second cut, this pattern reversed: STR (338.3 ± 32.3 kg DM kg^{-1} P) showed significantly lower PUE than P0 (397.5 ± 32.1 kg DM kg^{-1} P), while TSP (352.9 ± 43.6 kg DM kg^{-1} P) was intermediate. Cumulatively, TSP (267.8 ± 32.2 kg DM kg^{-1} P) showed significantly lower PUE than P0 (340.5 ± 33.3 kg DM kg^{-1} P), while STR (308.2 ± 20.8 kg DM kg^{-1} P) was intermediate and did not differ significantly from either treatment.

N uptake showed not only a strong temporal decline but also a shift in treatment differentiation (Figure 2C). In the first cut, STR (72.82 ± 4.81 kg ha^{-1}) had significantly lower N uptake than both P0 (78.98 ± 5.85 kg ha^{-1}) and TSP (79.52 ± 5.06 kg ha^{-1}), while P0 and TSP did not differ significantly from each other. The lower N uptake in STR could at least partly be related to the fertilization regime, as in STR, the liquid N dose was reduced by the amount of N supplied with struvite (about 9.5 kg N ha^{-1}), whereas in P0 and TSP the full N dosage was supplied via liquid ammonium- and nitrate-N fertilizer. Notably, this lower N uptake in STR coincided with the highest DM yield in the first cut. In the second cut, N uptake decreased markedly across all treatments. N uptake remained significantly lower under STR (19.99 ± 1.90 kg ha^{-1}) than under P0 (21.84 ± 0.90 kg ha^{-1}), while TSP (20.70 ± 1.49 kg ha^{-1}) showed intermediate values and did not differ significantly from either treatment. When both cuts were summed, cumulative N uptake was significantly lower under STR (92.81 ± 5.80 kg ha^{-1}) than under P0 (100.82 ± 5.75 kg ha^{-1}), with TSP (100.23 ± 6.11 kg ha^{-1}) again taking an intermediate position.

3.1.3 Macronutrient concentrations in plant biomass

Macronutrient concentrations in plant biomass exhibited clear treatment- and cut-specific patterns, reflecting temporal shifts in nutrient availability and plant uptake (Figures 3A–F). Across all treatments, concentrations generally declined from the first to the second cut, although the magnitude of this decline and the persistence of treatment differences varied among elements. This pattern was particularly pronounced for N (Figure 3A). In the first cut, P0 (43166 ± 7783 mg kg^{-1}) and TSP (38502 ± 3308 mg kg^{-1}) showed significantly higher N concentrations than STR (32741 ± 2335 mg kg^{-1}), while not differing significantly from each other. P0 was located in the upper part of the optimal range and partly above it, and TSP also reached the upper range and partly exceeded the upper threshold, whereas STR remained within the optimal range. This pattern corresponds to the fertilization design, as N in P0 and TSP was supplied entirely via the liquid fertilizer at sowing, while in STR part of the N supply was provided via struvite and was therefore less readily available during early growth (see also section above on N uptake). By the second cut, N concentrations had declined markedly in all treatments and were below the optimal range throughout, with no significant differences remaining among treatments.

For P (Figure 3B), treatment separation in the first cut was even more distinct. TSP (4577 ± 636 mg kg^{-1}) showed significantly higher concentrations than both P0 (3410 ± 551 mg kg^{-1}) and STR (3479 ± 284 mg kg^{-1}), whereas P0 and STR did not differ significantly from each other. Under TSP, P concentrations were in the upper part of the optimal range, while P0 and STR were located around the lower threshold or below it. Thus, the more readily soluble P source clearly translated into higher plant P concentrations during the first growth phase, whereas P concentrations under STR remained comparable to those of the unfertilized control. In the second cut, P concentrations declined in all treatments and were predominantly below the optimal range. Under these conditions, STR (2977 ± 276 mg kg^{-1}) showed significantly higher concentrations than P0 (2530 ± 219 mg kg^{-1}), while TSP (2872 ± 391 mg kg^{-1}) remained intermediate and did not differ significantly from either treatment. For Mg (Figure 3C), all treatments were within the optimal range in the first cut, but P0 (2482 ± 103 mg kg^{-1}) and TSP (2609 ± 160 mg kg^{-1}) showed significantly higher concentrations than STR (2351 ± 154 mg kg^{-1}), while not differing significantly from each other. This could be related to the fertilization design, because Mg in P0 and TSP was supplied via the liquid fertilizer, whereas in STR no additional liquid Mg was applied, based on the assumption that struvite already supplied a sufficient amount of Mg in plant available form. In the second cut, Mg concentrations declined overall and approached the lower boundary of the optimal range, particularly under TSP (1874 ± 115 mg kg^{-1}). At the same time, treatment ranking shifted: STR (2195 ± 269 mg kg^{-1}) showed significantly higher concentrations than TSP, while P0 (2126 ± 133 mg kg^{-1}) remained intermediate and did not differ significantly from either treatment.

K, Ca, and S were supplied in equal amounts and chemical forms across all treatments and are therefore presented here primarily to describe plant nutrient status. Compared with the other nutrients, K remained at comparatively high levels in both cuts (Figure 3D). In the first cut, K concentrations were above the reported optimal range in all treatments and were significantly lower in STR than in P0 and TSP. In the second cut, K concentrations declined but remained around the upper boundary of the

10.3389/fagro.2026.1885332

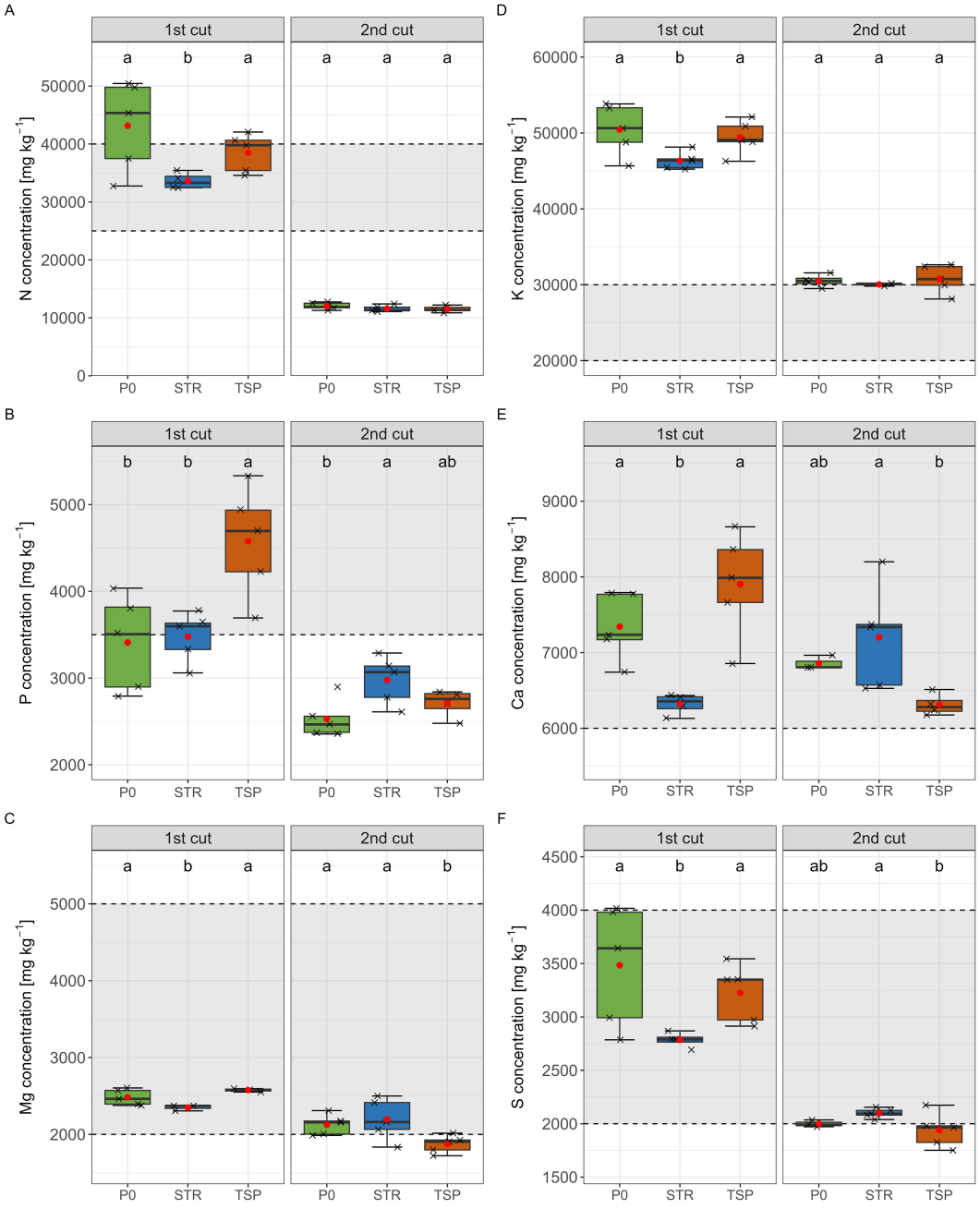

FIGURE 3
Nutrient concentrations in aboveground plant biomass for the first and second cut under the different phosphorus fertilization treatments (P0, STR, TSP). Panels show concentrations of **(A)** nitrogen (N), **(B)** phosphorus (P), **(C)** magnesium (Mg), **(D)** potassium (K), **(E)** calcium (Ca), and **(F)** sulfur (S). Grey shaded areas indicate optimal concentration ranges for adequate plant nutrient supply according to Finck (2007). Boxplots represent medians, interquartile ranges, and minimum–maximum values; individual symbols denote replicate observations, and red dots indicate treatment means. Different lowercase letters indicate significant differences among treatments within each cut according to Tukey's HSD test ($p < 0.05$).

reported optimal range across treatments, with no significant differences among treatments. Ca concentrations were within the reported optimal range in both cuts (Figure 3E). In the first cut, STR showed significantly lower Ca concentrations than P0 and TSP, while in the second cut STR showed significantly higher concentrations than TSP, with P0 occupying an intermediate position in both cuts. S concentrations were within or close to the reported optimal range in the first cut and declined towards or partly below the lower boundary in the second cut (Figure 3F). In the first cut, STR showed significantly lower S concentrations than P0 and TSP, whereas in the second cut STR showed significantly higher concentrations than TSP, while P0 again remained intermediate.

3.1.4 Micronutrient concentrations in plant biomass

Micronutrient concentrations in plant biomass varied mainly between cuts and, to a lesser extent, among treatments (Table 2). Because all treatments received identical micronutrient fertilization, the observed differences cannot be attributed to differences in

TABLE 2 Micronutrient concentrations (mg kg^{-1} DM) in aboveground plant biomass at the first and second cut under different phosphorus fertilization treatments (P0, STR, TSP).

Element	P0		STR		TSP		Optimal range (mg kg^{-1} DM)
	1st cut	2nd cut	1st cut	2nd cut	1st cut	2nd cut	
B	10 ± 2	14 ± 1.2	12.1 ± 1.0	15.1 ± 2.1	11.7 ± 1.0	13.0 ± 1.2	5-20
Cu	12.9 ± 2.3	5.7 ± 0.4	10.3 ± 0.7	6.0 ± 0.5	13.6 ± 2.4	5.4 ± 0.2	10-15
Fe	95.1 ± 13.1	62.3 ± 8.3	80.2 ± 5.5	66.7 ± 9.5	99.1 ± 14.7	62.3 ± 6.2	50-200
Mn	142 ± 16	445 ± 24	110 ± 17	435 ± 103	141 ± 16	398 ± 39	80-200
Mo	< LOQ	< LOQ	< LOQ	< LOQ	< LOQ	< LOQ	0.5-2
Zn	79.6 ± 19.3	38.8 ± 5.3	59.3 ± 4.6	37.4 ± 9.2	75.7 ± 10.9	36.2 ± 3.8	50-100

All treatments received identical micronutrient fertilization (B, Cu, Fe, Mn, Mo, Zn). Values are given as mean ± standard deviation. Lower and upper limits indicate optimal concentration ranges for plant nutrient supply.
DM, dry matter; LOQ, limit of quantification.

micronutrient input, but rather reflect treatment-specific effects on nutrient uptake, biomass formation, and nutrient dilution. Across treatments, the first cut generally showed an adequate micronutrient status for Cu, Fe, Mn, and Zn, with concentrations mostly within the reported optimal ranges. In the second cut, however, pronounced temporal shifts occurred. Cu and Zn declined markedly and fell below the optimal range in all treatments, whereas Mn increased strongly and exceeded the reported optimal range throughout. Fe remained within the reported optimal range in both cuts. B concentrations also remained within the reported optimal range across all treatments and cuts and consistently exceeded the critical value reported for dairy cow nutrition (< 3 mg kg^{-1} DM). Mo concentrations were below the analytical detection limit in all treatments and cuts and were therefore not evaluated further in relation to the reported optimal range. Treatment differences were more apparent in the first cut than in the second cut. In the first cut, P0 and TSP generally showed higher concentrations than STR for Cu, Fe, Mn, and Zn. B did not follow this pattern: its concentrations were slightly higher under STR and TSP than under P0 in the first cut and were highest under STR in the second cut. Relative to these treatment effects, variation between cuts was substantially stronger, indicating that temporal dynamics dominated the micronutrient composition. By the second cut, concentrations across treatments became more similar for several elements, while the overall pattern was mainly characterized by declining Cu and Zn and strongly increasing Mn concentrations.

3.1.5 Forage quality parameters

Forage quality parameters differed primarily between cuts, while treatment effects were more pronounced in the first than in the second cut (Figure 4). Across all treatments, CP concentrations closely followed the patterns observed for plant N concentrations (Figure 3), reflecting the well-established relationship between plant N concentration and crude protein content, given that proteins typically contain around 16% N. At the first cut, treatment effects were mainly expressed in CP, CF, WSC, and, to a lesser extent, to ELOS. CP was significantly higher under P0 compared to STR, while TSP showed intermediate values without significant differences to P0. CF was also significantly higher under P0, whereas STR and TSP showed lower and comparable values, indicating that CP and CF did not exhibit a strictly inverse relationship across treatments. WSC differed significantly among treatments, with highest concentrations under STR, significantly lower values under P0 and intermediate values under TSP. ELOS showed a weaker treatment differentiation, with significantly higher values under STR than under P0, while TSP remained intermediate and did not differ significantly from either treatment. In the second cut, CP declined across all treatments and no longer differed significantly, consistent with the convergence in plant N concentrations (Figure 3). Instead, treatment differences shifted mainly towards structural and carbohydrate-related parameters. CF showed significant variation among treatments, with lower values under TSP, while WSC remained significantly differentiated and highest under TSP. In contrast, ELOS did not differ significantly among treatments in the second cut.

3.2 Root parameters assessed by X-ray µCT

3.2.1 Root volume

Differences in root volume among treatments were generally small and restricted mainly to the first cut (Figures 5A–D). In the finest root fraction (0 – 0.5 mm), STR showed a significantly lower root volume than P0, whereas TSP remained intermediate and did not differ significantly from either treatment (Figure 5A). In the intermediate (> 0.5–1 mm) and coarse (> 1 mm) root classes, no significant treatment differences were detected in the first cut, although TSP showed numerically higher values than P0 and STR, though differences were not statistically significant (Figures 5B, C). This pattern was reflected in total root volume, where TSP showed significantly higher values than P0, while STR again occupied an intermediate position (Figure 5D). By the second cut, root volume had increased across all treatments and root classes, but no significant treatment differences were observed. In the finest root fraction, P0 showed numerically higher values, whereas in the coarse fraction TSP showed numerically higher values, though none of these differences were statistically significant, while the intermediate class showed only small differences among treatments (Figures 5A–C). Total root volume was also higher overall than in the first cut and showed broad overlap among P0, STR, and TSP (Figure 5D). Thus, treatment effects on root

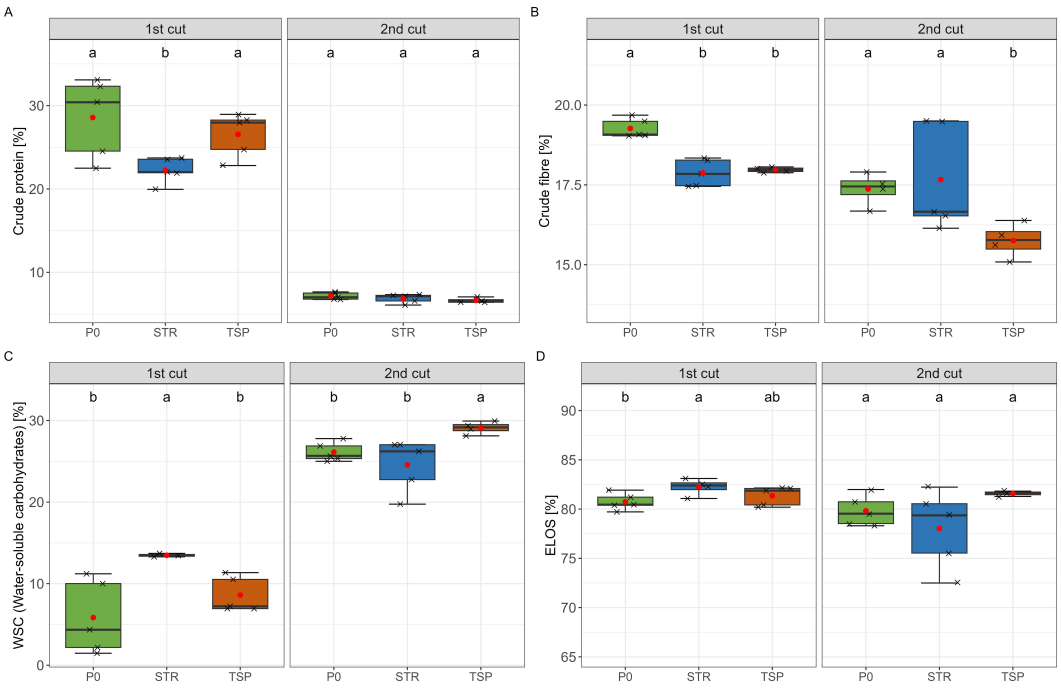

FIGURE 4
Forage quality parameters determined by near-infrared spectroscopy (NIRS) in aboveground biomass for the first and second cut under the different phosphorus fertilization treatments (P0, STR, TSP). Panels show **(A)** crude protein (CP), **(B)** crude fiber (CF), **(C)** water-soluble carbohydrates (WSC), and **(D)** enzymatic digestibility of organic matter (ELOS). Boxplots represent medians, interquartile ranges, and minimum–maximum values; symbols indicate individual replicates. Different lowercase letters denote significant differences among treatments within each cut according to Tukey's HSD test ($p < 0.05$).

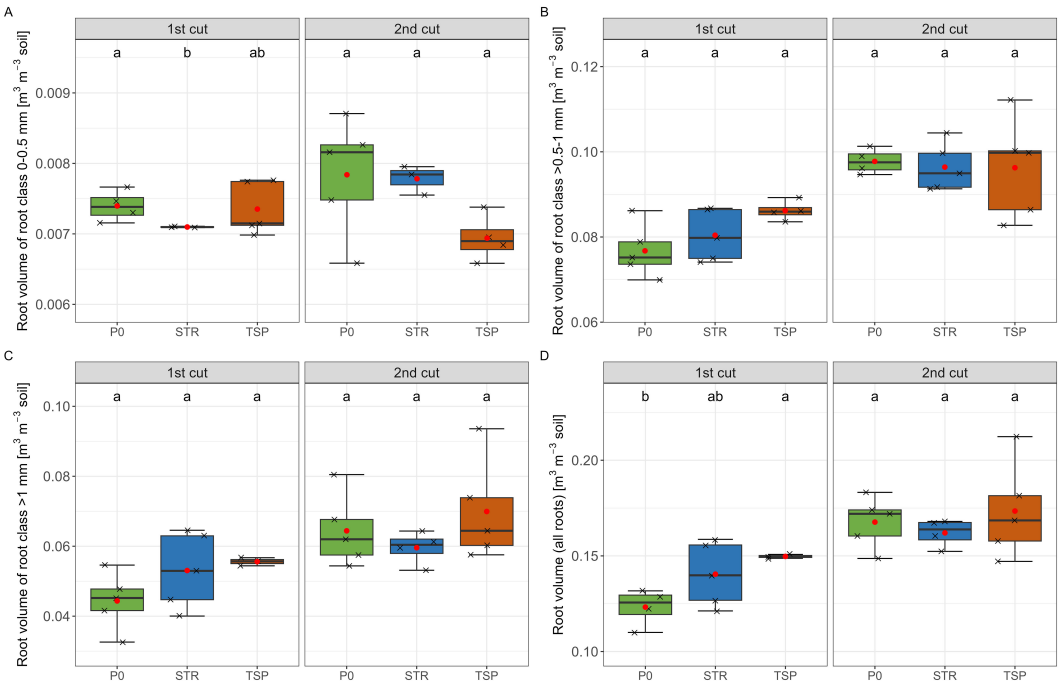

FIGURE 5
Root volume distribution across root size classes for the first and second cut under the different P fertilization treatments (P0, STR, TSP) assessed by X-ray micro-computed tomography analysis. Panels show root volume of **(A)** 0 – 0.5 mm, **(B)** > 0.5–1 mm, **(C)** > 1 mm diameter classes, and **(D)** total root volume (all roots). Boxplots represent medians, interquartile ranges, and minimum–maximum values; symbols indicate individual replicates. Different lowercase letters denote significant differences among treatments within each cut (Tukey HSD, $p < 0.05$).

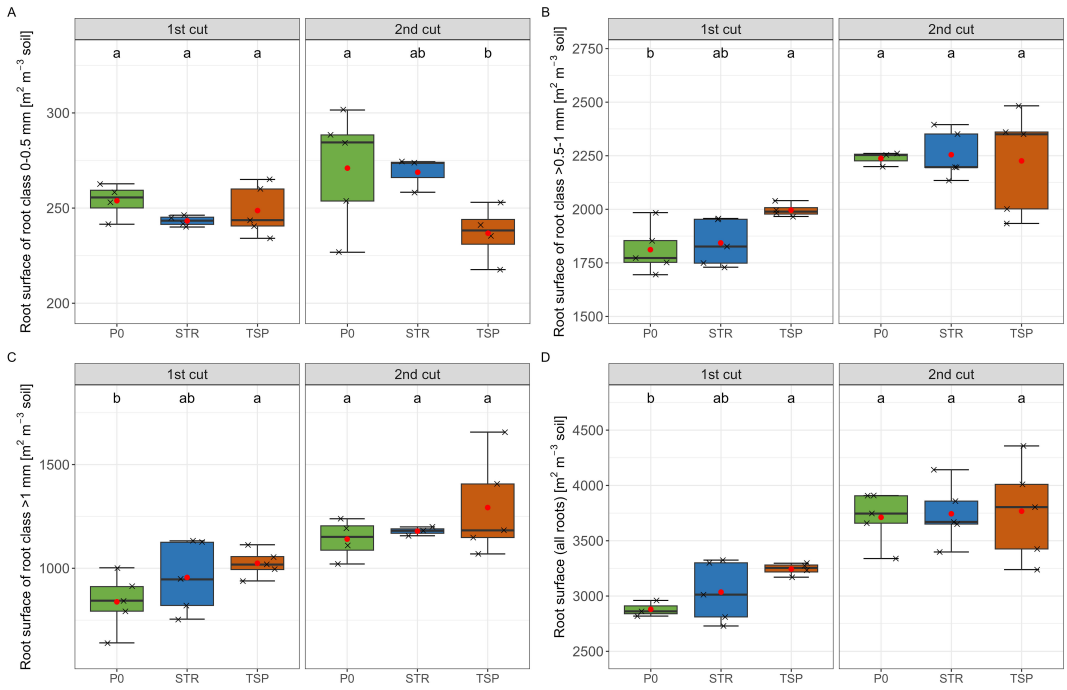

FIGURE 6
Root surface area distribution across root size classes for the first and second cut under the different P fertilization treatments (P0, STR, TSP) assessed by X-ray micro-computed tomography analysis. Panels show root surface of **(A)** 0 – 0.5 mm, **(B)** > 0.5–1 mm, **(C)** > 1 mm diameter classes, and **(D)** total root surface (all roots). Boxplots represent medians, interquartile ranges, and minimum–maximum values; symbols indicate individual replicates. Different lowercase letters denote significant differences among treatments within each cut (Tukey HSD, $p < 0.05$).

volume were mainly detectable at the earlier sampling stage and were no longer statistically distinguishable in the second cut.

3.2.2 Root surface

Treatment effects on root surface were expressed most clearly in the coarser root fractions and were most evident in the first cut (Figures 6A–D). No significant differences were observed in the finest root fraction (0 – 0.5 mm) at this stage, whereas TSP showed significantly greater root surface than P0 in both the > 0.5–1 mm and > 1 mm classes; STR remained intermediate in both cases (Figures 6B, C). The same pattern was reflected in total root surface, which was significantly higher under TSP than under P0 in the first cut (Figure 6D). By the second cut, root surface had increased overall, but treatment effects were largely no longer detectable. The only remaining significant difference occurred in the finest root fraction, where P0 showed greater root surface than TSP, while STR again remained intermediate (Figure 6A). In all other fractions, including total root surface, values overlapped broadly among treatments and no significant differences were observed. Overall, root surface responses were therefore strongest in the early growth phase and were mainly associated with differences in the coarser root fractions.

3.2.3 Vertical profiles of root volume and root surface

The vertical profiles of root volume and root surface showed a strong concentration of roots in the upper pot layers in both cuts (Figures 7A, B). The highest values occurred close to the surface, particularly within the upper 0–25 mm, where all treatments exhibited a similar overall profile shape. Across much of this upper profile zone, TSP showed numerically the highest values, whereas P0 and STR were closely aligned and alternated slightly depending on depth. Between 25 and 50 mm depth, the profiles separated more clearly. In this section, TSP generally maintained higher root volume and root surface than the other treatments, while P0 and STR remained closer together and changed rank locally. From 50 to 75 mm depth, the profiles became more similar again, indicating a reduced treatment effect in this middle part of the pot profile. Below 75 mm, a slight separation among treatments was visible once more, although this pattern was weaker and less consistent than in the upper and upper-middle sections.

4 Discussion

An integrated assessment of aboveground productivity, nutrient uptake and concentrations, forage quality and phenological development, together with belowground root system architecture, revealed distinct, treatment-specific response patterns. These patterns arose from the interaction between nutrient availability, plant demand, and root-mediated nutrient acquisition. By explicitly linking X-ray µCT-derived root traits with aboveground nutrient dynamics, this study demonstrates that the effects of fertilizer cannot be understood from shoot-based responses alone, but must be interpreted as the outcome of coordinated above- and belowground processes.

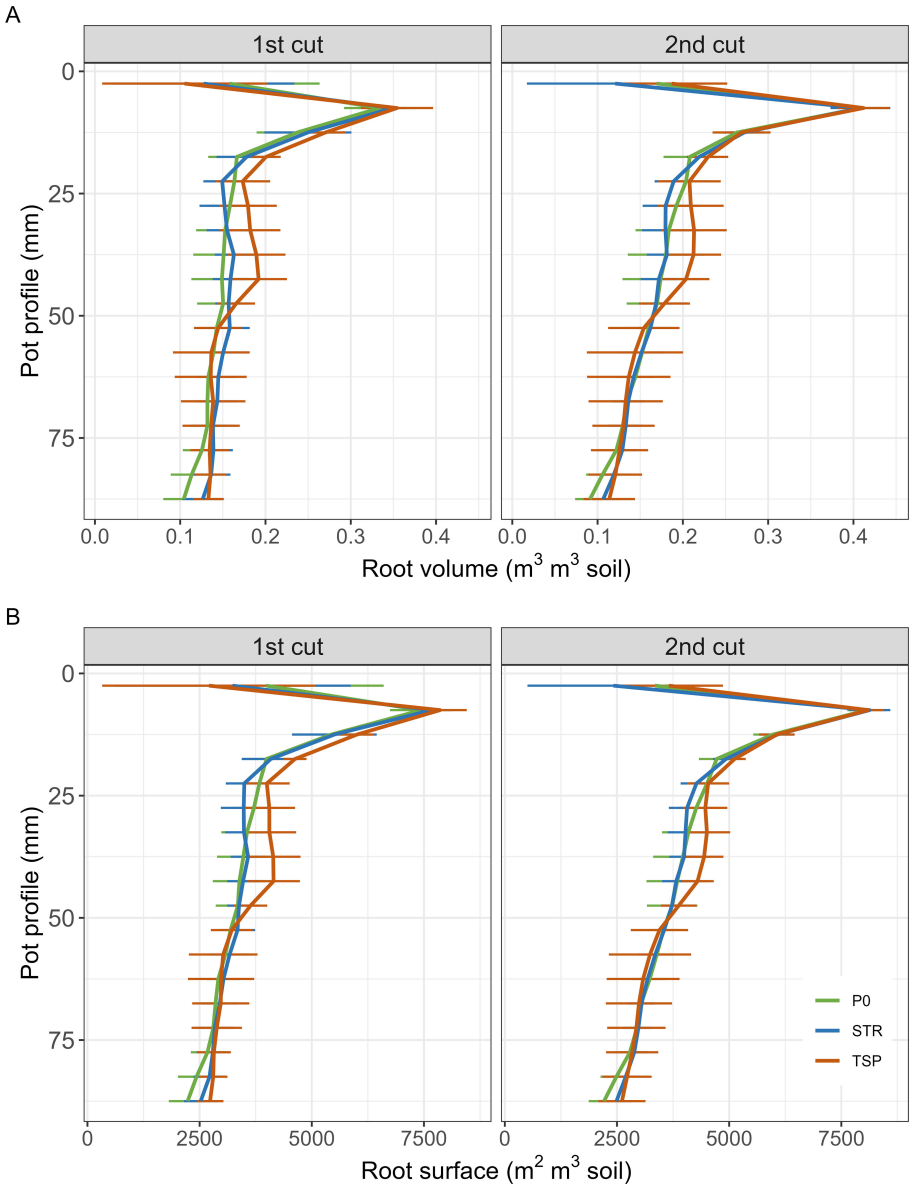

FIGURE 7
Vertical distribution of **(A)** root volume and **(B)** root surface along the pot profile for the first and second cut under the different P fertilization treatments (P0, STR, TSP), assessed by X-ray micro-computed tomography analysis. Lines represent mean values per depth increment; horizontal bars indicate variability among replicates. Root traits are shown as a function of depth (mm), illustrating treatment-specific differences in the upper soil layers and convergence with increasing depth.

4.1 Treatment-specific differences in aboveground plant development and productivity

The results partly support hypothesis (i). Treatment differences were expressed more clearly in nutrient uptake than in DM yield, whereas phenological development differed only slightly among treatments. Thus, aboveground productivity was not determined by nutrient supply alone, particularly during regrowth, when treatment effects on yield became less consistent than those on nutrient uptake.

A central finding is that DM yield did not mirror short-term nutrient availability in the same way as nutrient uptake. In the first cut, STR produced a significantly higher DM yield than P0 despite lower N uptake than P0 and TSP and lower P uptake than TSP, while DM yield did not differ significantly from TSP. Conversely, TSP showed the highest early P uptake, but this did not translate into the highest DM yield. These patterns indicate that nutrient uptake and biomass formation were not directly proportional under the present experimental conditions. Instead, the results suggest that first-cut biomass production was shaped by the temporal coordination of nutrient acquisition and biomass formation, so that higher nutrient uptake did not necessarily translate into higher DM yield during early growth. This interpretation is consistent with classical dilution concepts, according to which rapid biomass accumulation may coincide with comparatively lower tissue nutrient concentrations and lower nutrient uptake relative to yield (Jarrell and Beverly, 1981; Greenwood et al., 1990). The reversal between cuts, with STR showing the highest yield in the first cut but the lowest in the second, is nevertheless physiologically

plausible and consistent with general regrowth dynamics in perennial ryegrass and managed grassland systems. In grasses, a strong first harvest can constrain subsequent regrowth because post-defoliation growth depends on the amount of remaining assimilatory tissue, the mobilization of stored carbon and nitrogen reserves, the rebuilding of leaf area, and the restoration of nutrient uptake capacity. For perennial ryegrass, defoliation has been shown to reduce root growth and N uptake during regrowth and to increase reliance on internal remobilization, so that strong first growth can restrict subsequent regrowth when renewed uptake does not match demand (Davies, 1988; Lestienne et al., 2006; Thornton et al., 2000). In addition, recovery after defoliation in *Lolium perenne* has been shown to depend strongly on plant N reserve status, the balance between N remobilization and renewed mineral N uptake, and the dynamics of lamina regrowth (Louahlia et al., 2000). Likewise, regrowth and forage accumulation in *Lolium perenne* depend strongly on cutting interval and regrowth duration (Castro-Hernández et al., 2017). More recent studies support the same interpretation, linking post-defoliation herbage production to changes in root growth and water-soluble carbohydrate reserves and showing that DM production depends strongly on defoliation regime and rotation length (Turner et al., 2006; Tozer et al., 2024; Piña et al., 2025). Thus, the general pattern of high first-cut production followed by weaker regrowth is not unusual in grassland systems.

At the same time, the second-cut response should not be attributed to P source effects alone. By that stage, nutrient concentrations had declined strongly across treatments, particularly for N, and regrowth likely reflected the interaction of treatment-specific nutrient supply with post-defoliation physiology and declining nutrient availability. The marked decline in N uptake across all treatments in the second cut points to an overall insufficient N supply from the single basal fertilization applied at sowing. In retrospect, a repeated application of the basal nutrient solution after the first cut would have been advisable. Results of the second cut should therefore be interpreted with appropriate caution, as treatment differences may reflect the combined effects of P source and general N limitation rather than P source effects alone. This is important for interpreting the contrasting behavior of STR and TSP: although TSP promoted the highest early P uptake, the corresponding DM yield response remained intermediate, whereas STR combined intermediate P uptake with the highest first-cut DM yield. The uptake pattern therefore reflected fertilizer chemistry more directly than the yield pattern, especially for P, whose acquisition is strongly constrained by the low mobility of P in soil and by the temporal and spatial match between nutrient release and root activity (Lynch and Brown, 2008; Lynch, 2011; Talboys et al., 2016; Degryse et al., 2017).

A similar caution applies to the interpretation of N and Mg uptake. In the first cut, STR showed lower N uptake than P0 and TSP. This difference may have been influenced to some extent by the fertilization design, because a small proportion of N in STR was supplied with struvite rather than with liquid ammonium- and nitrate-N fertilizer. However, this fraction was small relative to total N input and is therefore unlikely to fully explain the observed treatment differences. Furthermore, Lunt et al. (1964) demonstrated that more than 90% of N from powdered, soil-incorporated struvite became plant-available within 30 days. Similarly, Mg uptake was lowest for STR in the first cut, which could be related to the different Mg source (water soluble MgCl2) in the P0 and TSP treatment (see Results section). While Watson et al. (2019) reported high plant availability of Mg from struvite in a pot trial with *Lolium multiflorum italicum L.*, the lower plant Mg concentration observed in our STR treatment suggests that Mg from struvite was not as quickly and fully plant available as the $MgCl_2$ provided to P0 and TSP in liquid form. However, taking into account the 14-day incubation period applied prior to sowing, it can be assumed that N and Mg from STR became largely plant-available during the course of the experiment. Thus, differences in N and Mg uptake are unlikely to be fully attributable to differential N and Mg availability alone. More importantly, the lower N uptake under STR coincided with the highest first-cut DM yield, again showing that N uptake and biomass formation were not directly proportional.

The contrasting PUE patterns reflect differences in P source characteristics and their interaction with plant demand. In the first cut, the significantly lower PUE under TSP despite its highest P uptake is consistent with luxury P consumption, whereby plants accumulate P beyond immediate metabolic requirements when supply is abundant (Vance et al., 2003; Richardson et al., 2011). The more gradual P release from struvite appears to have better matched plant demand, resulting in higher PUE. By the second cut, the pattern reversed, with STR showing the lowest PUE, likely reflecting the combined effect of reduced DM yield and general N limitation in the second cut. Cumulatively, TSP showed the lowest PUE, suggesting that its greater total P uptake was partly attributable to luxury consumption rather than productive P use.

A contribution of the pot system should also be considered, but not overstated. Restricted rooting volume may have limited the expression of treatment differences during later growth stages and may therefore have contributed to the convergence observed during regrowth. However, the main treatment patterns in the first cut, particularly the divergence between nutrient uptake and DM yield, remain biologically meaningful and should not be dismissed as artefacts of the experimental setup (McNickle, 2020).

4.2 Effects of treatment-specific nutrient supply on plant nutrient status and forage quality

Hypothesis (ii) was partly supported. Treatment-specific nutrient supply translated most clearly into differences in plant nutrient status for P, N, and Mg, and these differences were reflected in forage quality, particularly in the first cut. Across cuts, macronutrient concentrations showed pronounced temporal shifts, indicating that plant nutrient status was governed not only by fertilizer composition, but also by the interaction between nutrient availability, plant demand, biomass formation, and dilution. This is evident from the general decline in most macronutrient concentrations from the first to the second cut and from the partial re-ranking of treatments during regrowth.

In the first cut, concentration patterns for P, N, and Mg largely reflected the short-term supply characteristics of the treatments. TSP resulted in the highest plant P concentrations, consistent with its higher immediate solubility, whereas P concentrations under STR remained close to those of the unfertilized control. Although plant-available P was not determined after incubation in the present study, results from a previous experiment employing a comparable

experimental design[1] demonstrated that a two-week incubation with ground STR leads to a markedly smaller increase in CAL-extractable P concentrations than incubation with ground, fully water-soluble TSP. This pattern is likely to apply to the present study and is further supported by the significantly greater P uptake observed in the TSP treatment compared with the STR treatment at the first cut. However, the present experimental design may have attenuated treatment differences in initial P availability. To ensure homogeneous distribution within the substrate, finely ground P fertilizers were incorporated into the substrate and let equilibrate for two weeks. During this phase, a fraction of the water-soluble TSP-P may have been converted into less soluble forms through adsorption or precipitation, while simultaneously some STR-P may have dissolved into more readily available forms. Consequently, the observed differences in P uptake between TSP and STR may underestimate the contrasts expected under field conditions, where granulated fertilizers are typically incorporated into the soil shortly before or at sowing. A comparable contrast was observed for N, where P0 and TSP showed higher concentrations than STR, matching the greater immediate availability of liquid mineral N in these treatments. For Mg, P0 and TSP likewise showed higher concentrations than STR, consistent with the different Mg supply regime in STR. It is noteworthy, however, that the substrate used in this experiment was characterised by a high inherent Mg availability (150 mg Mg kg^{-1} in $CaCl_2$ extract, VDLUFA soil Mg level E), suggesting that Mg supply was not limiting in any treatment and that the observed concentration differences reflect supply-form effects rather than overall Mg deficiency. By the second cut, however, most concentrations had declined substantially, often approaching or falling below the lower limit of the reported optimal range. Under these conditions, plant nutrient status during re-growth appears to have been shaped less directly by immediate fertilizer composition than by the combined effects of previous uptake, biomass production, and nutrient dilution.

K, Ca, and S were supplied in equal amounts and chemical forms across all treatments. Differences in their plant concentrations therefore most likely reflect treatment-associated variation in plant composition, biomass formation, and dilution rather than direct effects of phosphorus fertilization. In this context, the first cut was characterized by concentrations generally within or close to the reported optimal ranges, whereas the second cut showed a broader decline towards lower concentration levels and a partial re-ranking of treatments. Thus, variation in K, Ca, and S is more appropriately interpreted as a response to temporal changes in plant nutrient status during regrowth than as a direct consequence of fertilizer-specific nutrient supply.

These differences in nutrient status were reflected most clearly in CP. CP closely followed plant N concentration in both cuts, as expected from the close biochemical relationship between tissue N and protein formation. In the first cut, CP was highest under P0, lower under STR, and intermediate under TSP, consistent with the lower early N availability in STR. From a feeding perspective, this distinction is relevant because forage for lactating dairy cows generally needs to contribute to diets formulated around moderate to high crude protein concentrations, commonly in the range of about 15 to 18% of DM depending on production level and ration composition (National Academies of Sciences, Engineering, and Medicine, 2016; Lavery et al., 2025). Against this background, the first-cut forage can still be regarded as valuable perennial ryegrass forage for dairy-oriented systems, whereas the second cut, with CP values only around 6 to 7% DM across treatments, falls clearly below the level required for lactating cows and would not represent adequate high-quality basal forage without substantial protein supplementation (Zeleke et al., 2025). For less demanding animal categories, however, such forage may still have value. Practical feeding guidelines for mature beef cows often place minimum dietary CP near 7 to 8% DM for maintenance-oriented conditions, although requirements rise with growth, gestation, and lactation (MSD Veterinary Manual, 2023; Oklahoma State University Extension, 2025).

Normally, CF increases as CP declines, and vice versa. In the present study, however, this inverse relationship was not consistently expressed across treatments. In the first cut, P0 combined the highest CP with the highest CF, whereas STR showed both lower CP and lower CF, indicating that treatment effects on CP cannot be explained simply by structural dilution or a straightforward maturity effect. Instead, the data suggest treatment-specific shifts in plant composition and carbon–nitrogen partitioning. This interpretation is supported by the WSC pattern: in the first cut, STR showed the highest WSC, suggesting that reduced short-term N availability was associated with a greater accumulation of soluble carbohydrates. The combination of lower CP and higher WSC under STR is therefore consistent with a shift in biomass composition away from N-rich compounds and towards soluble carbon fractions. This may also help explain the slightly higher ELOS under STR than under P0, as a greater concentration of readily fermentable carbohydrates likely improved the energy-related quality of the biomass despite its lower protein status (Humphreys, 1989). By the second cut, CP had converged at uniformly low levels, whereas CF and WSC still differed among treatments, with TSP showing the lowest CF and the highest WSC. This indicates that forage quality during regrowth was determined less by protein nutrition and more by carbohydrate and structural fractions. Such patterns are consistent with broader forage-quality literature showing that CP, fiber fractions, soluble carbohydrates, and digestibility often respond jointly to nutrient supply and harvest timing, but not necessarily through a simple one-dimensional trade-off between protein and fiber (Olszewska, 2021; Šidlauskaitė et al., 2024; Wróbel et al., 2025; Irisarri et al., 2025). However, the agronomic relevance of these quality responses depends on their combination with biomass production. When DM yield and forage quality were considered together, the most favourable treatment depended on the cut. In the first cut, STR provided the best yield–quality combination, with the highest DM yield, high WSC, low CF, and higher ELOS than P0, despite lower CP. In the second cut, TSP was more favourable, combining a yield comparable to P0 with the highest WSC and low CF. Thus, STR mainly improved early biomass production, whereas TSP showed the more balanced regrowth quality.

Micronutrient concentrations were influenced much more strongly by cut than by treatment. Because all treatments received identical micronutrient fertilization, the decline in Cu and Zn and the strong

1 Keßeler, P., Bloem, E., and Kratz, S. (n.d.) Development of a standard pot trial for the agronomic evaluation of recycled phosphorus fertilizers using struvite and ryegrass (Lolium multiflorum Lam.). (submitted).

increase in Mn from the first to the second cut are best explained by cut-specific physiological and dilution effects rather than by differences in micronutrient supply. The strong increase in Mn is most likely related to reduced biomass dilution during regrowth rather than to changes in Mn supply, which was identical across all treatments. The fact that treatment effects were more visible in the first cut but diminished in the second further supports the conclusion that temporal dynamics dominated micronutrient composition. Overall, hypothesis (ii) was therefore supported most clearly for P, N, Mg, and the associated forage quality traits, whereas K, Ca, S, and micronutrients mainly reflected general plant nutrient status and regrowth-related changes in plant composition.

4.3 Root system development and vertical root distribution in response to treatment-specific nutrient supply

Hypothesis (iii) was partly supported. Root system development responded to treatment-specific nutrient supply, but these responses were strongest in the first cut and were not expressed uniformly across all root size classes or both sampling dates. Thus, the data indicate treatment effects on root development, but they do not support a simple or consistent compensatory root response under reduced P availability.

The clearest treatment differences occurred in the first cut, when nutrient availability differed most strongly among treatments. Under these conditions, TSP showed greater total root volume and total root surface than P0, while STR was mostly intermediate. This pattern is consistent with the greater short-term P availability under TSP and suggests that readily accessible P promoted stronger early root system development, particularly in the coarser root fractions. Such a pattern is consistent with the general concept that P acquisition in grasses depends strongly on root-mediated soil exploration and on the spatial match between root deployment and localized nutrient-rich zones (Lynch and Brown, 2008; Lynch, 2011, 2019), which is also reflected here by the stronger early root development under TSP and the concentration of root volume and root surface in the upper pot layers. The intermediate position of STR is likewise compatible with its slower nutrient-release pattern, as struvite-derived P is less immediately available than water-soluble mineral P. In this context, Ahmed et al. (2016) showed that struvite dissolution depends strongly on root proximity and rhizosphere processes, which provides a plausible explanation for the weaker early root response under STR than under TSP.

At the same time, the results do not support a clear and uniform compensatory increase in root development under reduced P availability. In the first cut, neither P0 nor STR showed consistently greater root volume or root surface in the finest diameter class, although such a response might have been expected under lower P supply based on general concepts of phosphorus-acquisition strategies in grasses (Hill et al., 2006; Lyu et al., 2016; Chen et al., 2018). By the second cut, P0 tended to show higher values in the finest root fraction, and the significantly greater root surface in the 0 – 0.5 mm class relative to TSP may indicate some increase in absorptive root structures under lower P availability. However, this pattern was limited to a specific root class and sampling date and therefore provides only restricted evidence for a delayed compensatory response. Overall, the data suggest that reduced P availability influenced fine-root development only weakly and not in a consistent manner across the whole root system.

By the second cut, most treatment differences in total root volume and total root surface had disappeared, despite an overall increase in root system size across treatments. This indicates that fertilizer effects on root architecture were most pronounced during early establishment and became less distinct during regrowth. The later convergence likely reflects both biological and experimental factors. Biologically, continued root proliferation across treatments reduced relative differences over time. Experimentally, the restricted rooting volume of the pot system may also have limited the further expression of treatment-specific root responses during later growth stages. However, this does not invalidate the early treatment effects; rather, it suggests that second-cut root patterns should be interpreted more cautiously than those observed in the first cut.

The vertical profiles add an important spatial dimension to these results. Across both cuts, root volume and root surface were strongly concentrated in the upper pot layers, with the highest values in the upper 0–25 mm and a broadly similar overall profile shape among treatments. This indicates that all treatments primarily exploited the upper substrate layers, which is consistent with the importance of topsoil foraging for the acquisition of relatively immobile nutrients such as P (Lynch and Brown, 2008; Lynch, 2011). Within this shared pattern, TSP generally maintained the highest values in the upper and upper-middle profile, particularly between about 25 and 50 mm, whereas P0 and STR remained closer together. The profile data therefore support the interpretation that rapidly available P under TSP promoted stronger early root proliferation in the upper rooting zone, rather than inducing a marked redistribution of roots towards deeper layers.

4.4 Agronomic implications

The findings, when considered as a whole, show that fertilizer effects were governed less by total P input than by the form and timing of nutrient release and the resulting plant response. Under the conditions of this pot experiment, TSP produced the strongest short-term P effect, whereas STR followed a slower but still agronomically effective response pathway. In this respect, STR did not behave as a direct substitute for TSP, but rather as a functionally distinct P source with a different temporal and more root-dependent mode of action (Talboys et al., 2016; Degryse et al., 2017; DeLucca-Agrelo et al., 2026). This distinction is relevant not only agronomically, but also from a circular-economy perspective, because struvite contributes to recovering and returning phosphorus from secondary sources to agricultural production. At the same time, these implications should be interpreted with caution, as the experiment was conducted in a homogenized sandy substrate under pot conditions, with a comparatively small pot size necessitated by X-ray μCT scanning, and with finely ground fertilizer materials. The present results therefore provide evidence primarily for contrasting functional behavior of STR and TSP rather than a direct basis for management recommendations. Further studies in larger pots and, most importantly, under field conditions are needed to test whether the differences observed here in nutrient delivery, regrowth, and root development persist under practical grassland management.

5 Conclusions

The agronomic performance of P fertilizers in grassland systems depends not only on the amount of P applied but also on how the release of nutrients from the fertilizer aligns with plant demand over time. In this study, STR and TSP produced distinct response patterns in *Lolium perenne* despite receiving the same amount of P. These findings show that fertilizer performance was determined less by total P input than by the timing and mode of nutrient availability and by the way this interacted with plant growth and root development over time. Accordingly, STR should not be viewed simply as a direct substitute for TSP, but rather as a functionally distinct recycled P source with a different temporal mode of action. The clearest differences among treatments occurred during early growth, whereas later responses were less distinct and must be interpreted more cautiously, particularly because nutrient concentrations, especially N, declined strongly during regrowth, indicating an N deficit that also influenced subsequent plant responses. A central contribution of this study is therefore that fertilizer effects could not be adequately understood from aboveground traits alone. The integration of shoot responses with X-ray µCT-derived root traits provided additional insight into how P source may influence the timing of root system development, complementing the aboveground nutrient dynamics, though treatment effects on root traits were not uniform across root size classes or sampling dates. At the same time, these conclusions need to be considered within the limits of the experimental setup. The study was conducted in a homogenized sandy substrate under pot conditions, with a comparatively small pot size necessitated by X-ray µCT scanning, and with finely ground fertilizer materials. The present results therefore provide evidence primarily for contrasting functional behavior rather than a direct basis for management recommendations. Further studies in larger pots and, most importantly, under field conditions are needed to test whether the patterns observed here persist under practical grassland management. Finally, the results demonstrate that the important question is not whether STR mimics TSP but rather whether its unique pattern of nutrient delivery can be strategically employed in more sustainable grassland fertilization systems.

Data availability statement

The raw data supporting the conclusions of this article will be made available by the authors, without undue reservation.

Author contributions

KK: Conceptualization, Data curation, Formal analysis, Funding acquisition, Investigation, Methodology, Project administration, Resources, Software, Supervision, Validation, Visualization, Writing – original draft, Writing – review & editing. MSR: Formal analysis, Investigation, Validation, Visualization, Writing – review & editing. PK: Formal analysis, Investigation, Resources, Validation, Writing – review & editing. SK: Conceptualization, Investigation, Validation, Writing – review & editing. EB: Investigation, Resources, Validation, Writing – review & editing.

Funding

The author(s) declared that financial support was received for this work and/or its publication. This work was supported by the project CiNURGi (Circular Nutrients for a Sustainable Baltic Sea Region; project number C049), funded by the Interreg Baltic Sea Region Programme 2021–2027 and co-funded by the European Union through the European Regional Development Fund (ERDF).

Acknowledgments

The authors gratefully acknowledge Cheryl Marie Cordeiro, PhD, and Erik Sindhøj, PhD, of RISE Research Institutes of Sweden for their project coordination within the CiNURGi project. We are also grateful to Anja Voges for her highly valuable technical support in the preparation and conduct of the pot experiment, including substrate preparation and filling, fertilizer application, irrigation, and harvesting. We thank the laboratory team for sample processing, laboratory organization, fertilizer solution preparation, microwave-assisted digestion, ICP-OES measurements, and CN analyses, with special thanks to Sophia Albert, Kathrin Goltz, Sandra Hübner, Edda Oelker, and Sabine Schuckel for their particularly valuable support. Special thanks also go to Merle Alex for carrying out the NIRS measurements. The authors further thank Jan-Martin Voigt for his support with watering. Finally, we thank Joachim Clemens of Soepenberg GmbH for providing the struvite fertilizer used in this study within the framework of the CiNURGi project.

Conflict of interest

The author(s) declared that this work was conducted in the absence of any commercial or financial relationships that could be construed as a potential conflict of interest.

Generative AI statement

The author(s) declared that generative AI was not used in the creation of this manuscript.

Any alternative text (alt text) provided alongside figures in this article has been generated by Frontiers with the support of artificial intelligence and reasonable efforts have been made to ensure accuracy, including review by the authors wherever possible. If you identify any issues, please contact us.

Publisher's note

References

Ahmed, S., Klassen, T. N., Keyes, S., Daly, M., Jones, D. L., Mavrogordato, M., et al. (2016). Imaging the interaction of roots and phosphate fertiliser granules using 4D X-ray tomography. *Plant Soil* 401, 125–134. doi: 10.1007/s11104-015-2425-5

Bengough, A. G., Bransby, M. F., Hans, J., McKenna, S. J., Roberts, T. J., and Valentine, T. A. (2006). Root responses to soil physical conditions; growth dynamics from field to cell. *J. Exp. Bot.* 57, 437–447. doi: 10.1093/jxb/erj003

Castro-Hernández, H., Domínguez-Vara, I. A., Morales-Almaráz, E., and Huerta-Bravo, M. (2017). Chemical composition, mineral content and *in vitro* digestibility from ryegrass (Lolium perenne) in relation to the cutting interval and growing season. *Rev. Mex. Cienc. Pecu.* 8, 201–210.

Chen, Y., Rengel, Z., Palta, J., and Siddique, K. H. M. (2018). Efficient root systems for enhancing tolerance of crops to water and phosphorus limitation. *Indian Journal of Plant Physiology* 23 (4), 689–696. doi: 10.1007/s40502-018-0415-3

Cordell, D., Drangert, J.-O., and White, S. (2009). The story of phosphorus: global food security and food for thought. *Global Environ. Change* 19, 292–305. doi: 10.1016/j.gloenvcha.2008.10.009

Davies, A. (1988). "The regrowth of grass swards," in *The Grass Crop: The Physiological Basis of Production* (London, UK: Chapman and Hall), 85–127.

Degryse, F., Baird, R., Da Silva, R. C., and McLaughlin, M. J. (2017). Dissolution rate and agronomic effectiveness of struvite fertilizers – effect of soil pH, granulation and base excess. *Plant Soil* 410, 139–152. doi: 10.1007/s11104-016-2990-2

Deinert, L., Ikoyi, I., Egeter, B., Forrestal, P., and Schmalenberger, A. (2023). Short-term impact of recycling-derived fertilizers on their P supply for perennial ryegrass (Lolium perenne). *Plants* 12, 2762. doi: 10.3390/plants12152762

DeLucca-Agrelo, F., Condron, L., and Moir, J. (2026). Assessment of the relative agronomic effectiveness of struvite fertilizer in a temperate grassland. *Nutr. Cycling Agroecosyst.* 132, 14. doi: 10.1007/s10705-025-10465-x

Finck, A. (2007). *Pflanzenernährung und Düngung in Stichworten*. *6th* ed. (Stuttgart: Gebrüder Borntraeger).

Gao, Y., Zhang, Z., Zeng, F., and Ma, X. (2023). Root morphological and physiological traits are committed to the phosphorus acquisition of the desert plants in phosphorus-deficient soils. *BMC Plant Biol.* 23, 188. doi: 10.1186/s12870-023-04178-y

Greenwood, D. J., Lemaire, G., Gosse, G., Cruz, P., Draycott, A., and Neeteson, J. J. (1990). Decline in percentage N of C3 and C4 crops with increasing plant mass. *Ann. Bot.* 66, 425–436. doi: 10.1093/oxfordjournals.aob.a088044

Hammond, J. P., and White, P. J. (2008). Sucrose transport in the phloem: integrating root responses to phosphorus starvation. *J. Exp. Bot.* 59, 93–109. doi: 10.1093/jxb/erm221

Hartig, F. (2016). "DHARMa: residual diagnostics for hierarchical (multi-level/mixed) regression models," in *Cran: Contributed Packages*. (Vienna, Austria: R Foundation for Statistical Computing (CRAN)).

HELCOM (2021). *Baltic Sea Action Plan—2021 Update*. (Helsinki: Baltic Marine Environment Protection Commission).

Hill, J. O., Simpson, R. J., Moore, A. D., and Chapman, D. F. (2006). Morphology and response of roots of pasture species to phosphorus and nitrogen nutrition. *Plant Soil* 286, 7–19. doi: 10.1007/s11104-006-0014-3

Humphreys, M. O. (1989). Water-soluble carbohydrates in perennial ryegrass breeding: III. Relationships with herbage production, digestibility and crude protein content. *Grass Forage Sci.* 44, 423–430. doi: 10.1111/j.1365-2494.1989.tb01942.x

Irisarri, J. G. N., Texeira, M. A., Harris, P., and Pembleton, K. G. (2025). Satellite-based monitoring of forage quality in grasslands of the United Kingdom using sentinel-2 data and random forest regression. *Front. Vet. Sci.* 12. doi: 10.3389/fvets.2025.1678123

Jarrell, W. M., and Beverly, R. B. (1981). "The Dilution Effect in Plant Nutrition Studies," in *Advances in Agronomy*. Ed. N. C. Brady (New York, USA: Academic Press), 197–224.

Koebernick, N., Weller, U., Huber, K., Schlüter, S., Vogel, H.-J., Jahn, R., et al. (2014). In situ visualization and quantification of three-dimensional root system architecture and growth using X-ray computed tomography. *Vadose Zone J.* 13, vzj2014-03. doi: 10.2136/vzj2014.03.0024

Kratz, S., Vogel, C., and Adam, C. (2019). Agronomic performance of P recycling fertilizers and methods to predict it: a review. *Nutr. Cycling Agroecosyst.* 115, 1–39. doi: 10.1007/s10705-019-10010-7

Kuka, K., Illerhaus, B., Fox, C. A., and Joschko, M. (2013). X-ray computed microtomography for the study of the soil–root relationship in grassland soils. *Vadose Zone J.* 12, vzj2013. 01.0014. doi: 10.2136/vzj2013.01.0014

Kuka, K., and Joschko, M. (2024). Grassland management intensity determines root development, soil structure, and their interrelationship: Results of a regional study of Leptosols in the Swabian Alps. *Grassland Res.* 3, 171–186. doi: 10.1002/glr2.12077

Lavery, A., Craig, A., Gordon, A. W., White, A., Barkley, N., and Ferris, C. P. (2025). Reducing dietary crude protein levels while meeting metabolizable protein requirements: Performance of dairy cows over a full lactation period. *J. Dairy Sci.* 108, 1451–1473. doi: 10.3168/jds.2024-25405

Lenth, R. (2023). "emmeans: estimated marginal means, aka least-squares means_," in *R Package Version 1.8. 5*. (Vienna, Austria: R Foundation for Statistical Computing (CRAN)).

Lestienne, F., Thornton, B., and Gastal, F. (2006). Impact of defoliation intensity and frequency on N uptake and mobilization in Lolium perenne. *J. Exp. Bot.* 57, 997–1006. doi: 10.1093/jxb/erj085

Louahlia, S., Laine, P., Thornton, B., Ourry, A., and Boucaud, J. (2000). The role of N-remobilisation and the uptake of NH4+ and NO3-by Lolium perenne L. in laminae growth following defoliation under field conditions. *Plant Soil* Wallingford, UK: CABI Publishing 220, 175–187. doi: 10.1023/a:1004728327955

Lunt, O. R., Kofranek, A. M., and Clark, S. B. (1964). Nutrient availability in soil, availability of minerals from magnesium ammonium phosphates. *J. Agric. Food. Chem.* 12, 497–504. doi: 10.1021/jf60136a005

Lynch, J. P. (2011). Root phenes for enhanced soil exploration and phosphorus acquisition: tools for future crops. *Plant Physiol.* 156, 1041–1049. doi: 10.1104/pp.111.175414

Lynch, J. P. (2019). Root phenotypes for improved nutrient capture: an underexploited opportunity for global agriculture. *New Phytol.* 223, 548–564. doi: 10.1111/nph.15738

Lynch, J. P., and Brown, K. M. (2008). "Root strategies for phosphorus acquisition," in *The Ecophysiology of Plant-Phosphorus Interactions* (Dordrecht, The Netherlands: Springer), 83–116.

Lyu, Y., Tang, H., Li, H., Zhang, F., Rengel, Z., Whalley, W. R., et al. (2016). Major crop species show differential balance between root morphological and physiological responses to variable phosphorus supply. *Front. Plant Sci.* 7, 1939. doi: 10.3389/fpls.2016.01939

McConville, J., Drangert, J.-O., Tidåker, P., Neset, T.-S., Rauch, S., Strid, I., et al. (2015). Closing the food loops: guidelines and criteria for improving nutrient management. *Sustainability: Sci. Pract. Policy* 11, 33–43. doi: 10.1080/15487733.2015.11908144

McGillycuddy, M., Popovic, G., Bolker, B. M., and Warton, D. I. (2025). Parsimoniously fitting large multivariate random effects in glmmTMB. *J. Stat. Softw.* 112, 1–19. doi: 10.18637/jss.v112.i01

McNickle, G. G. (2020). Interpreting plant root responses to nutrients, neighbours and pot volume depends on researchers' assumptions. *Funct. Ecol.* 34, 2199–2209. doi: 10.1111/1365-2435.13517

Mooney, S. J., Pridmore, T. P., Helliwell, J., and Bennett, M. J. (2012). Developing X-ray computed tomography to non-invasively image 3-D root systems architecture in soil. *Plant Soil* 352, 1–22. doi: 10.1007/s11104-011-1039-9

MSD Veterinary Manual (2023). Feeding and nutritional management of beef cattle. Available online at: https://www.msdvetmanual.com/management-and-nutrition/nutrition-beef-cattle/feeding-and-nutritional-management-of-beef-cattle (Accessed May 15, 2026).

National Academies of Sciences, Engineering, and Medicine (2016). *Nutrient Requirements of Beef Cattle*. *8th* rev. ed. (Washington, DC, USA: The National Academies Press). doi: 10.17226/25806

Oklahoma State University Extension (2025). Nutrient requirements of beef cattle. Available online at: https://extension.okstate.edu/fact-sheets/print-publications/e/e-974-2025-nutrient-beef-requirements-a.pdf (Accessed May 15, 2026).

Olszewska, M. (2021). Effects of cultivar, nitrogen rate and harvest time on the content of carbohydrates and protein in the biomass of perennial ryegrass. *Agronomy* 11, 468. doi: 10.3390/agronomy11030468

Piña, L. F., Merino, V. M., Navarro, M. J., Mella, F. C., Lucero, C., Seguel, G., et al. (2025). Rotation length and defoliation intensity effects on dry matter production and botanical composition in perennial ryegrass–white clover and multispecies pastures. *Agronomy* 15, 2097. doi: 10.3390/agronomy15092097

Poetsch, E. M., Resch, R., and Krautzer, B. (2016). Variability of yield and forage quality between three heading groups of english ryegrass (Lolium perenne L.) during the first growth/Variabilität von Ertrag und Futterqualität zwischen drei Reifegruppen von

Englischem Raygras (Lolium perenne L.) im Verlauf des ersten Aufwuchses. *Die Bodenkultur: J. Land Manag. Food. Environ.* 67, 69–75. doi: 10.1515/boku-2016-0007

Richardson, A. E., Lynch, J. P., Ryan, P. R., Delhaize, E., Smith, F. A., Smith, S. E., et al. (2011). Plant and microbial strategies to improve the phosphorus efficiency of agriculture. *Plant Soil* 349, 121–156. doi: 10.1007/s11104-011-0950-4

Ros, M. B. H., Deyn, G. B., Koopmans, G. F., Oenema, O., and van Groenigen, J. W. (2018). What root traits determine grass resistance to phosphorus deficiency in production grassland? *J. Plant Nutr. Soil Sci.* 181, 323–335. doi: 10.1002/jpln.201700093

Schmitt Rahner, M., and Kuka, K. A reproducible X-ray micro-computed tomography workflow for segmenting roots, pores, and water-associated phases in a homogeneous plant-growth substrate. (in preparation).

Shen, Q., Wen, Z., Dong, Y., Li, H., Miao, Y., and Shen, J. (2018). The responses of root morphology and phosphorus-mobilizing exudations in wheat to increasing shoot phosphorus concentration. *AoB Plants* 10, ply054. doi: 10.1093/aobpla/ply054

Šidlauskaitė, G., Toleikienė, M., and Kadžiulienė, Ž. (2024). Comparison of productivity and quality of three perennial ryegrass cultivars and their mixture in response to nitrogen fertilization and grass-legume mixtures. *Plants* 13, 3130. doi: 10.3390/plants13223130

Talboys, P. J., Heppell, J., Roose, T., Healey, J. R., Jones, D. L., and Withers, P. J. A. (2016). Struvite: a slow-release fertiliser for sustainable phosphorus management? *Plant Soil* 401, 109–123. doi: 10.1007/s11104-015-2747-3

Teramoto, S., Takayasu, S., Kitomi, Y., Arai-Sanoh, Y., Tanabata, T., and Uga, Y. (2020). High-throughput three-dimensional visualization of root system architecture of rice using X-ray computed tomography. *Plant Methods* 16, 66. doi: 10.1186/s13007-020-00612-6

Thornton, B., Millard, P., and Bausenwein, U. (2000). "Reserve formation and recycling of carbon and nitrogen during regrowth of defoliated plants," in *08519945*. (Wallingford, UK: CABI Publishing). doi: 10.1079/9780851994529.0085

Tozer, K. N., Greenfield, R. M., Cameron, C. A., Upsdell, M. P., and Hume, D. E. (2024). Effect of three defoliation frequency treatments and drought on perennial ryegrass herbage and root growth and water-soluble carbohydrate reserves. *Grassland Res.* 3, 347–363. doi: 10.1002/glr2.12105

Turner, L. R., Donaghy, D. J., Lane, P. A., and Rawnsley, R. P. (2006). Effect of defoliation interval on water-soluble carbohydrate and nitrogen energy reserves, regrowth of leaves and roots, and tiller number of cocksfoot (Dactylis glomerata L.) plants. *Aust. J. Agric. Res.* 57, 243–249. doi: 10.1071/ar05130

Vance, C. P., Uhde-Stone, C., and Allan, D. L. (2003). Phosphorus acquisition and use: critical adaptations by plants for securing a nonrenewable resource. *New Phytol.* 157, 423–447. doi: 10.1046/j.1469-8137.2003.00695.x

van Nguyen, L., and Stangoulis, J. (2019). Variation in root system architecture and morphology of two wheat genotypes is a predictor of their tolerance to phosphorus deficiency. *Acta Physiol. Plant* 41, 109. doi: 10.1007/s11738-019-2891-0

Waddell, H. A., Simpson, R. J., Ryan, M. H., Lambers, H., Garden, D. L., and Richardson, A. E. (2017). Root morphology and its contribution to a large root system for phosphorus uptake by rytidosperma species (wallaby grass). *Plant Soil* 412, 7–19. doi: 10.1007/s11104-016-2933-y

Watson, C., Clemens, J., and Wichern, F. (2019). Plant availability of magnesium and phosphorus from struvite with concurrent nitrification inhibitor application. *Soil Use Manage.* 35, 675–682. doi: 10.1111/sum.12527

Wen, Z., Li, H., Shen, Q., Tang, X., Xiong, C., Li, H., et al. (2019). Tradeoffs among root morphology, exudation and mycorrhizal symbioses for phosphorus-acquisition strategies of 16 crop species. *New Phytol.* 223, 882–895. doi: 10.1111/nph.15833

Wickham, H., Averick, M., Bryan, J., Chang, W., McGowan, L. D., François, R., et al. (2019). Welcome to the tidyverse. *J. Open Source Softw.* 4, 1686. doi: 10.21105/joss.01686

Withers, P. J. A., Sylvester-Bradley, R., Jones, D. L., Healey, J. R., and Talboys, P. J. (2014). Feed the crop not the soil: rethinking phosphorus management in the food chain. *Environ. Sci. Technol.* 48, 6523–6530. doi: 10.1021/es501670j

Wróbel, B., Zielewicz, W., and Paszkiewicz-Jasińska, A. (2025). Improving forage quality from permanent grasslands to enhance ruminant productivity. *Agriculture* 15, 1438. doi: 10.3390/agriculture15131438

Wu, A., Fang, Y., Liu, S., Wang, H., Xu, B., Zhang, S., et al. (2021). Root morphology and rhizosheath acid phosphatase activity in legume and graminoid species respond differently to low phosphorus supply. *Rhizosphere* 19, 100391. doi: 10.1016/j.rhisph.2021.100391

Yan, Y., Kallikazarou, N. I., Nisiforou, O., Shang, Q., Fu, D., Antoniou, M. G., et al. (2025). Phosphorus recovery through struvite crystallization from real wastewater: bridging gaps from lab to market. *Bioresour. Technol.* 427, 132408. doi: 10.1016/j.biortech.2025.132408

Zeleke, A. W., DiMonaco, N. J., Lawther, K., Lavery, A., Ferris, C., Moorby, J., et al. (2025). Reducing crude protein content in the diet of lactating dairy cows improved nitrogen-use-efficiency and reduced N excretion in urine, whilst having no obvious effects on the rumen microbiome. *J. Anim. Sci. Biotechnol.* 16, 113. doi: 10.1186/s40104-025-01240-7